文章编号：1001-9014(2022)06-0972-08

DOI:10.11972/j.issn.1001-9014.2022.06.005

High speed uncooled MWIR infrared HgCdTe photodetector based on graded bandgap structure

SANG Mao-Sheng[1,2], XU Guo-Qing[1], QIAO Hui[1], LI Xiang-Yang[1*]

(1. Key Laboratory of Infrared Imaging Materials and Detectors, Shanghai Institute of Technical Physics, Chinese Academy of Sciences, Shanghai 200083, China;
2. University of Chinese Academy of Sciences, Beijing 100049, China)

Abstract: A high-speed room-temperature mid-wave infrared HgCdTe photodetector based on graded bandgap structure was reported. This study explores a n-on-p homojunction structure on epitaxial HgCdTe, which achieves a total response time of 1.33 ns (750 MHz) under zero bias voltage at 300 K, which is faster than commercial uncooled MCT photovoltaic photodetectors and MWIR HgCdTe APDs under high reverse bias. The analysis based on one-dimensional equations shows that compositional grading in the absorber layer can form built-in electric field and the transport mechanism of carriers is changed, the model is confirmed by the comparisons of different graded HgCdTe photodetectors. Thereby, this work facilitates design of the high-speed HgCdTe MWIR detectors, and provides a promising method to optimize the ultrafast MWIR infrared photodetectors.

Key words: HgCdTe, high speed, mid-wave infrared, component gradient

基于梯度能带结构的高速非制冷中波红外HgCdTe探测器

桑茂盛[1,2], 徐国庆[1], 乔 辉[1], 李向阳[1*]

(1. 中国科学院上海技术物理研究所 红外成像材料与器件重点实验室,上海 200083;
2. 中国科学院大学,北京 100049)

摘要:报道了基于梯度能带结构的高速室温中波红外HgCdTe器件,器件设计为n-on-p同质结结构,在300 K的零偏压条件下达到了1.33 ns(750 MHz)的总的响应时间,相对于非制冷的碲镉汞器件和工作于高偏压下的碲镉汞APD器件响应速度有所提高。基于一维模型的分析表明,吸收层中的组分梯度可以形成内置电场并改变了载流子的输运特性,该模型由不同组分梯度的HgCdTe器件的实验对比验证。因此,此项工作优化了高速HgCdTe中波红外探测器的设计,并为设计超快中波红外光电探测器提供了一种可行的思路。

关 键 词:碲镉汞;高速;中波红外;组分梯度

Introduction

High-performance uncooled mid-wavelength infrared (MWIR) photodetectors are of great significance in communication, sensing, as well as other military and commercial applications [1,3]. In some special applications, such as frequency comb spectroscopy techniques and free optical communication systems, ultrafast photodetectors operated at room temperature are required as important components[2]. In recent years, quantum cascade laser (QCL) and interband cascade laser (ICL) operating at 3-5um wavelength have been used as light sources in spectroscopy detection and so on [4-5]. Meanwhile, these applications especially correlated with detection require high-speed photodetectors operated in mid-wave infrared band, which are not fully developed.

Currently, HgCdTe-based photodetector is one of the most promising detection options due to the superior merits of tunable bandgap, high absorption, high sensitivity, small size, low power consumption and light weight [6]. HgCdTe has made great contribution to the progress of devices such as photoconductance (PC), photovoltaic (PV) and other emerging structures in decades[7], but some devices such as n-Barrier-n detector

Received date: 2022-03-22, **revised date**: 2022-09-02 **收稿日期**:2022-03-22,**修回日期**:2022-09-02
Foundation items: Supported by the National Key Research and Development Program of China (2021YFA0715501)
Biography: SANG Mao-Sheng(1995-), male, Fuyang China, Ph. D. Research area involve Semiconductor material and device
E-mail: sangmaosheng@mail.sitp.ac.cn
* **Corresponding author**: E-mail: lixy@mail.sitp.ac.cn

is difficult to fabricate compared with photoconductance or photovoltaic MCT photodetectors [8]. The planar or mesa structure of MCT PC and PV photodetector is usually adopted due to the aspects of easy fabrication and high reproducibility. Especially, planar HgCdTe photodetector show excellent flexibility in manufacturing units and focal plane arrays, and can play a crucial role in ultrafast photodetectors due to the high mobility and broad infrared wave band.

In HgCdTe photodetectors, photoconductors can achieve a relative high frequency response due to the fast decay of the photogenerated carriers in the absorber region. However, the response time of photoconductors is limited by the minority carrier life time of HgCdTe, and the frequency response can be just below MHz range. The photovoltaic detector utilizes the electric field due to the formation of p-n junction, which can separate the photogenerated carriers in the absorber region and transport the carries to the contacts, so the response time of photovoltaic detector can be much shorter than photoconductors.

Response time and dark current are the key indicators of ultrafast HgCdTe photodetectors. However, the research on the response time and frequency response of MCT photodetector is not fully studied. For LWIR band, high performance HgCdTe photodiodes with more than 30% QE and 1 GHz bandwidth have been achieved in cryogenic temperature (77 K) [9] in 1980s, but the bandwidth is calculated by RC-limited time. HgCdTe mid-wave infrared (MWIR) n-on-p homogeneous structure has been developed for high-speed photodetectors, where the electron mobility is approximately an order of magnitude larger than hole mobility, and the ultrafast photodetector is available by the optimization of structure design, especially, HgCdTe APD structure is mostly used to achieve high bandwidth.

Researchers have reported the various applications of HgCdTe MWIR e-APDs, which focused on the dark current, the bandwidth and the avalanche gain. For instance, Rothman *et al*. successfully manufactured a MWIR e-APD at CEA LETI in 2007, which measured a risetime of $t_{10\text{-}90}$=88 ps and a fall time of $t_{90\text{-}10}$=2.4 ns, the GBW is recorded as 723 GHz [10]. Perrais *et al*. studied the impulse response in frontside-illuminated mid-wave infrared HgCdTe e-APDs, the rise time of $t_{10\text{-}90}$ =70 ps is noted at M = 3500 with reverse bias of 12 V, the corresponding RC-limited bandwidth is 600 MHz, which yields a new absolute recorded in gain-bandwidth product of GBW = 2.1 THz [11]. Rothman *et al*. then reported a backside-illuminated short-wave infrared HgCdTe avalanche photodiodes (APDs) with maximum bandwidth of the diodes to about 600 MHz in 2014 [12]. Beck *et al*. reported an HgCdTe e-APD which developed for lidar receivers, the measured bandwidth is 6.8 MHz at 11 V reversed bias but was more than adequate for 1μs pulse detection [13]. The bandwidth of HgCdTe photodiodes is calculated in different ways, but the measurement of photocurrent under ultrafast pulse lasers in time domain can be applied to compare the response speed of different devices. Typically, the MWIR e-APD has high gain based on avalanche mechanism at high bias, but the HgCdTe APDs need to be operated at linear mode, in which large bias voltage indicates high gain and large bandwidth while large dark current. The HgCdTe APDs also need to work at cryogenic temperature to get high gain-band width (GBW), which limited the application in some scenes without expensive cooling equipment.

In this paper, we reported a n-on-p homojunction photodiode based on epitaxial HgCdTe, which achieves fast response at 300 K. The HgCdTe photodetector has a fast response time of 1.33 ns (BW=750 MHz) under zero bias voltage at room temperature. The device is fabricated by vapor epitaxial HgCdTe material. The composition grading is inherent to epitaxial process [14], and the diffusion length of minority carriers can be increased by introducing component gradients in the absorbent layer, which benefits the improvement of the responsivity of device. The minority carrier diffusion length is correlated with built-in electric field formed by composition gradient[15], and the quantum efficiency is changed. The built-in electric field can be improved for larger grading, which is essential for the transport of minority carriers generated in absorber layers, and it is beneficial to use this mechanism in the fabrication of high-speed devices.

HgCdTe n-on-p photodiodes fabricated by LPE and VPE HgCdTe materials exhibit obvious advantages in response speed under pulse light source at room temperature, but the frequency response of photodiodes is quite different, the response time is estimated to be 8.7 ns and 1.33 ns, respectively. We establish a one-dimensional model to clarify the underlying transport mechanisms of different graded HgCdTe photodiodes. Device performance analysis revealed that the validity of our model can be confirmed. This study provides a route towards achieving ultrafast MWIR HgCdTe photodetectors and may find various kinds of applications in the promising MWIR regime.

1 Device structure and characterization

The cross-section views of different graded front side illuminated n-on-p HgCdTe photodetector are shown in Figs. 1(a-b), respectively. The photodetector is designed to operate in mid-wave infrared band based on graded HgCdTe materials. Figure 1(c) illustrates the energy band structure of conventional planar HgCdTe photodetector without composition gradient. However, p-type $Hg_{1-x}Cd_xTe$ epilayers are grown on CdZnTe substrates, the Cd composition is graded from the CdZnTe substrate to the top layer. The bandgap is special in p-type HgCdTe materials with composition gradient. Figure 1(d) shows the varying bandgap in p-type layers, leading to the built-in electric field in the graded layers.

The liquid phase epitaxy material is adopted to fabricate photodiodes with Cd component fraction of 0.3 at the top surface of the layer. Vapor phase epitaxy material is applied for larger grading, the composition is varied from 0.57 to 0.31 across the epilayer, and the cross-sectional transmission electron microscopy (TEM) image of

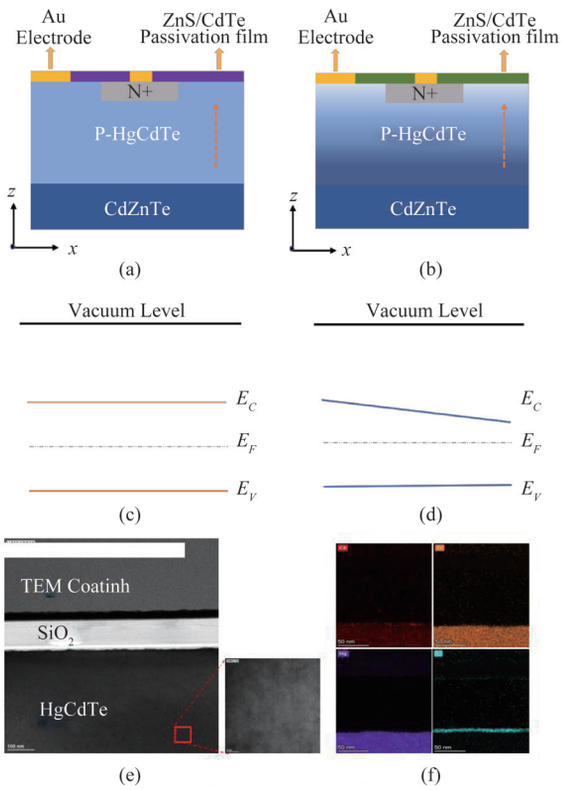

Fig. 1 Schematic of the graded HgCdTe photodetector and energy band structure (a) schematic diagram of HgCdTe photodetector, (b) cross-section view of the graded HgCdTe photodetector. Energy band profiles of p-type MCT material, (c) without grading, (d) with grading, (e) cross-sectional TEM image of the graded HgCdTe materials, and (f) EDS mappings of the structure
图1 HgCdTe光伏器件和能带结构示意图 (a) HgCdTe器件的二维示意图, (b) 梯度能带结构的HgCdTe器件的二维示意图, (c)无组分梯度,(d)有组分梯度的p型碲镉汞材料的能带图,(e)梯度组分的HgCdTe材料的TEM横截面图, (f) 材料的EDS测试图

VPE materials is depicted in Fig. 1(e), which shows the crystal lattice and the graded multilayer structure of the MCT material. Energy-dispersive X-ray spectrometry (EDS) mapping in Fig. 1(f) shows that there is no Au element in the MCT materials, the p-type layer is dominated by Hg vacancies, the Cd, Hg, and Te atoms are uniformly distributed in the epitaxy layer.

In graded HgCdTe photodiodes, when the photodetector is irradiated by the MWIR laser, the electron-hole pairs will be generated in absorber layer, the built-in electric filed associated with the bandgap will contribute to the transport of generated carriers. The carriers in the absorber region will transport to the depletion region, and the ion implantation induced electric filed separate electron-hole pairs rapidly. For planar MCT photovoltaic devices, the electron will dominate the carrier transport in p-type layer, the electron mobility is much higher in contrast to hole mobility, so the generated minority carriers are readily evacuated from the absorber region under the built-in electric field, and ultimately leading to the improvement of the frequency performance of the photodetectors.

2 Device optoelectronic properties and modeling

P-type HgCdTe material is doped by Hg vacancies with a concentration of 1×10^{16} cm^{-3} grown by the liquid phase epitaxy and vapor phase epitaxy method. The gradient of Cd composition is different in MCT photodetectors based on LPE and VPE materials. Figure 2(a) shows the roughly fabrication process of device. N-type layer was manufactured by boron (B) ion implantation, which would generate more Hg interstitials to occupy Hg vacancies to form n-type dopant. The doping concentrations in between p-type and n-type layer form the p-n junction region. A 200 nm thick ZnS/CdTe double passivation layer is deposited after ion implantation of the diodes. Finally, the Au electrode was deposited after lithography and etching processes, and Ohmic contact was formed in sequence.

Figure 2(b) shows that the spectral responses of HgCdTe photodetectors and background are measured with a Fourier-transform infrared spectroscope to calculate the normalized spectral response of device. The response spectrums of LPE and VPE MCT photodetectors indicate that the cutoff wavelength of devices is approximately 4.6 μm. Figure 2(c) shows the output characteristics under 2000 nm illumination of different laser powers, the generation of photocarriers shifts the *I-V* curve downward, indicates that the generated photocurrent increases with the increase of the incident power, inset of Fig. 2(c) illustrates the photovoltaic effect, the electron-hole pairs generate under excitation of photos are separated by built-in electric field and collected by contacts. Figure 2(d) is the current-voltage (*I-V*) curve of the graded MCT photodetector based on LPE material measured at 300 K without laser illumination. The dark current of MCT detectors under room temperature is large because Shockley - Read - Hall (SRH) and Auger Recombination have significant effect on total dark current due to the strong temperature dependence [16].

To clarify the mechanism of built-in electric field associated with grading Cd composition in HgCdTe photodetector, the composition gradient is measured through Fourier-Transform Infrared (FTIR) spectra, which is shown in Fig. 2(f). The vapor phase epitaxy grown HgCdTe material is removed in succession by erosion in bromide solution. The FTIR spectra is record after etching of HgCdTe top layer, the dependent dielectric function model of HgCdTe graded structures is used to calculate the distribution of Cd composition in epitaxy layers, the bandgap profile can also be determined [17]. More specifically, the graded epitaxy layers are divided into piles of thin sublayers correlated with fixed composition in this model, and the Cd composition in top layer is roughly obtained by fitting the FTIR spectra. Energy bandgap profiles is validated and will be further analyzed in one-dimensional numerical model.

A theoretical investigation of the performance of n-on-p $Hg_{1-x}Cd_xTe$ homojunction photodiodes with a linear gradient in composition is presented. The composition

profile and band diagram of graded n-on-p HgCdTe photodetector are depicted in Fig. 2(e). The Cd mole fraction changes along the p-type region, which results in variations of optoelectronic properties in HgCdTe photodiodes. The spatial dependence of Cd composition is associated with properties like the bandgap, the absorption coefficient, the electron lifetime and built-in electric field in detail. One-dimensional equations including Poisson equation, the carrier's continuity equation and current transport equation are used to demonstrate composition dependences with built-in electric filed in graded p-type absorber region. As described by Rosenfeld *et al*[18] in linearly graded n-type HgCdTe photodiodes, the composition profile in the n-type layer is linear and results in a constant electric field. In n-on-p HgCdTe photodiodes, the optical and electrical coefficient have spatial depen-

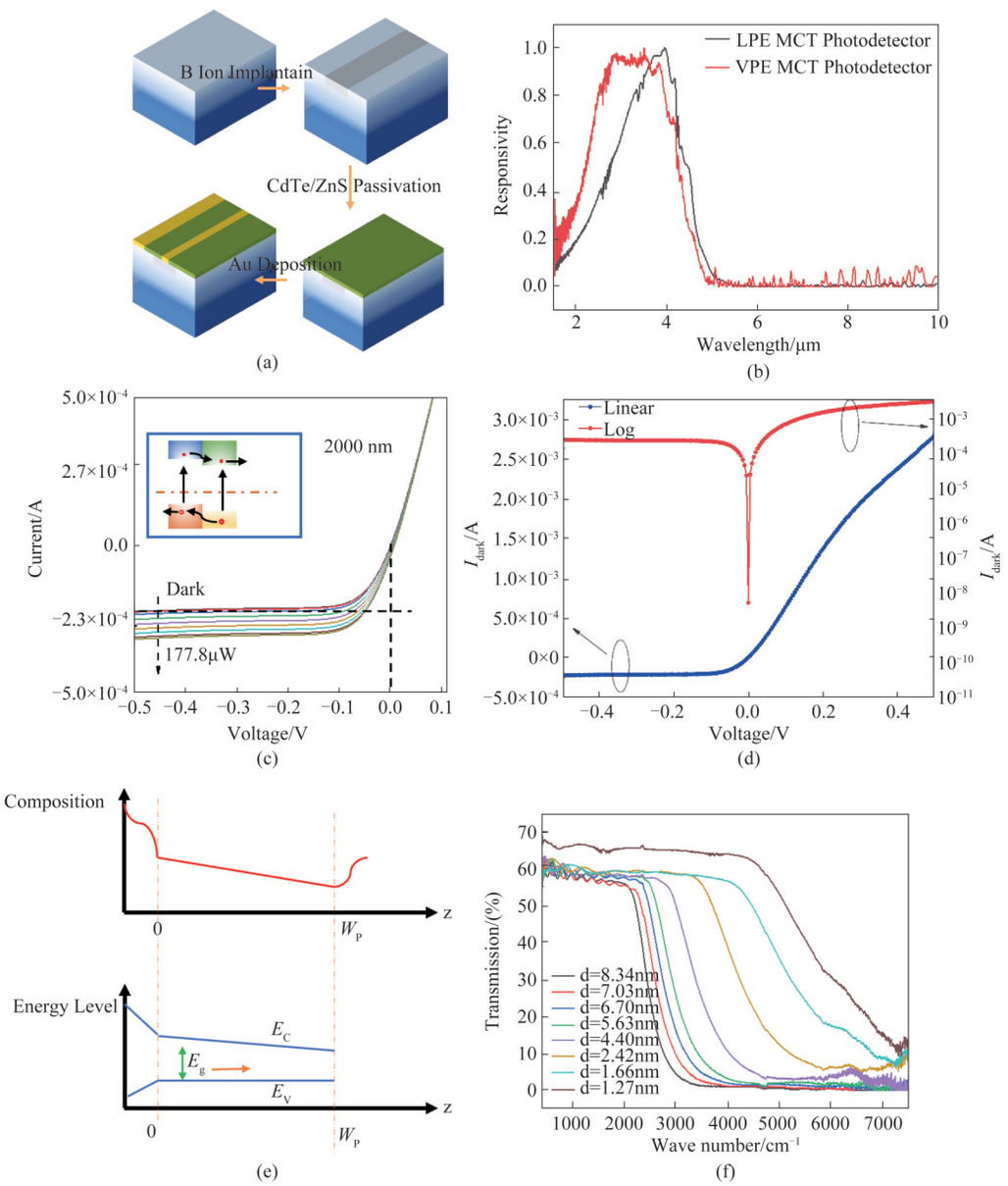

Fig. 2 Device fabrication and the measurement in detail (a) Fabrication process of HgCdTe photodetector, (b) The normalized spectral response spectrum of MCT photodetector based on graded LPE and VPE materials at 300 K, the absorption cut-off wavelength is broadened to 4.6um, (c) *I-V* curves of LPE MCT photodetector for incident laser powers from 0 to 177.8 μW. The inset describes the photovoltaic mechanism for detecting mid-infrared radiation, (d) Linear plots (bule) and logarithmic plots (red) of dark current in LPE MCT photodetector as a function of bias voltage, (e) The schematic model description of the composition profile and the band diagram associated with the photodiode, and (f) FTIR spectra recorded after continuous etching of the HgCdTe epilayer (*d* = thickness of epilayer from the CdZnTe substrate after wet etching)

图2 器件的制备和电学性能测试表征 (a) 碲镉汞器件的制备流程示意图, (b) 室温下基于LPE和VPE材料制作的碲镉汞器件的归一化响应光谱,响应截止波长约为4.6 μm, (c) 室温下LPE 碲镉汞器件在入射激光功率为0至177.8 μW时的*I-V*曲线,(d) 室温下LPE 碲镉汞器件的暗电流与偏压的线性和对数关系图示,(e) 器件组分和能带的原理性建模图示, (f) 连续湿法腐蚀HgCdTe外延层后测得的FTIR光谱(d为腐蚀后的HgCdTe外延层厚度)

dence with linear p-type absorber region. The bandgap $E_g(z)$ and absorption coefficient $\alpha(z, \lambda)$ are taken to calculate the distribution of the minority carriers $N(z)$ in p-type region [19]. The built-in electric field resulting from the compositional gradient is given as $E_{\text{built-in}}$ to illustrate the improvement of response time. The quantum efficiency η_{graded} is also considered in graded p-type layers. The minority carrier lifetime is determined by an Auger 7 mechanism in n-on-p diodes and the dark current is dominated by the diffusion and drift current in this model. Carrier transport speed in the graded energy-gap HgCdTe photodiodes is improved by built-in electric field, which is confirmed by LPE and VPE graded HgCdTe photodiodes in sequences.

For $Hg_{1-x}Cd_xTe$, the composition and temperature dependence on band gap (eV) is determined by [20]

$$E_g = -0.302 + 1.93\cdot x + 5.35\times 10^{-4}\cdot T\cdot(1-2x) - 0.81\cdot x^2 + 0.132\cdot x^3 \quad . \quad (1)$$

The energy bandgap grading across the p-type graded region is expressed as

$$\Delta E_g = E_g^{z=0} - E_g^{z=W_p} \quad . \quad (2)$$

The energy-gap gradient and built-in electric field resulting from the compositional gradient are given by

$$E_{\text{built-in}} = \frac{\Delta E_g}{W_p} \quad , \quad (3)$$

$$\varepsilon_{\text{built-in}} = \frac{1}{q}\frac{\Delta E_g}{W_p} \quad . \quad (4)$$

As schematically depicted in Fig. 2(e), band gap decreases linearly from $z=0$ to $z=W_p$ as composition gradient varies in absorber region, W_p is the thickness of the p-type epilayer. A linear gradient over the p-region of the n-on-p homojunction structure is assumed. In VPE HgCdTe materials, a total of eight gradient profiles are calculated by etching the top layers the Cd composition at $z=0$ is fixed at 0.57, while the composition at $z=W_p$ is 0.31. The magnitude of ΔE_g is correlated with the composition gradient in LPE and VPE materials, and the built-in electric field can be different, respectively. The distribution of minority carriers dominates the dark and photocurrent in n-on-p HgCdTe photodiodes, the concentration of electrons Δn_z can be obtained by solving steady-state continuity equation under illumination conditions, which should be expressed as,

$$D_n\frac{\partial \Delta n_z}{\partial z^2} + \mu_n\varepsilon_{\text{built-in}}\frac{\partial \Delta n_z}{\partial z} - \frac{\Delta n_z}{\tau_n} + G_L(z,\lambda) = 0 \quad , \quad (5)$$

where D_n is the diffusion coefficient and μ_n is the mobility of minority carriers, the relationship between them can be depicted as Einstein relation

$$\frac{D_n}{\mu_n} = \frac{k_0 T}{q} \quad , \quad (6)$$

where q is the electronic charge, h is Planck's constant, and k_0 is Boltzmann's constant. The boundary condition of solving continuity Eq. 5 is

$$\Delta n_{z=W_p} = n_{z=W_p}(e^{qV/kT} - 1) \quad , \quad (7)$$

$n_{z=Wp}$ is the electron concentration at $z=W$p, V is the applied voltage, the minority carries generation rate $G_L(z, \lambda)$ is related with the depth of absorber layer and wavelength of infrared radiation. The absorption coefficient $\alpha(z, \lambda)$ varies with composition in HgCdTe epilayers, $G_L(z, \lambda)$ can be expressed as

$$G_L(z,\lambda) = -\frac{d\phi(z)}{dz} = \alpha(z,\lambda)\phi_0 e^{-\int_0^z \alpha(u,\lambda)du} \quad , \quad (8)$$

where ϕ_0 is the value of the photon flux at $z=0$, $G_L(z, \lambda)$ can be quite complicated due to the varied absorption coefficient, and the calculation of G_L should follow the given average absorption coefficient and cutoff wavelength of infrared radiation. The solution of steady continuity Eq. 5 under boundary conditions is

$$\Delta n_z = (A_1 + A_{1z})e^{(-m-N)z} + (A_2 + A_{2z})e^{(-m+N)z} \quad . \quad (9)$$

The terms resulting from the built-in electric field, "m" and "N," have a direct influence on minority carries. A_1 and A_2 are coefficients of the surface recombination velocity S_n at $z=0$ and can be calculated when $\Delta n_z = 0$ at $z=W_p$ correlated with Eq. 7

$$m = \frac{E_{\text{built-in}}}{2k_0 T} \quad , \quad (10)$$

$$N = \sqrt{m^2 + \left(\frac{1}{L_n}\right)^2} \quad , \quad (11)$$

$$L_n = \sqrt{D_n\tau_n} \quad , \quad (12)$$

$$A_{1z} = \frac{1}{2ND_n}\int_0^z G_L e^{(m+N)u}du \quad , \quad (13)$$

$$A_{1z} = -\frac{1}{2ND_n}\int_0^z G_L e^{(m-N)u}du \quad . \quad (14)$$

The photogenerated carriers are regarded as the main components in minority carriers. The analysis based on above one-dimensional equations clarifies the optical performance under illumination. The total current includes photocurrent and dark current, where the dark current is induced by thermally generated minority carriers under room temperature. The photocurrent behaviors need to be analyzed in detail and photocurrent density J_λ can be obtained by

$$J_\lambda = qD_n\left(\frac{d\Delta n_z}{dz} + 2m\Delta n_z\right)|z = W_p \quad . \quad (15)$$

The quantum efficiency of graded n-on-p HgCdTe photodiodes η is analyzed due to its influence on detectivity D^* of photodetector. The detectivity depend on quantum efficiency η_{graded} with zero-bias resistance area product R_0A. The theoretical expression of D^* and η_{graded} under operating wavelength λ is given by

$$D^* = \frac{q\eta\lambda}{hc}\sqrt{\frac{R_0A}{4k_0T}} \quad , \quad (16)$$

$$\gamma_n = \frac{S_nL_n}{D_n} \quad , \quad (17)$$

$$G_1 = \frac{1}{\phi_0}\int_0^{W_p} G_L e^{-(m+N)u}du \quad , \quad (18)$$

$$G_2 = \frac{1}{\phi_0}\int_0^{W_p} G_L \mathrm{e}^{-(m-N)u}\mathrm{d}u \quad , \quad (19)$$

$$\eta_{\mathrm{graded}} = \frac{J_\lambda}{q\phi_0} \quad , \quad (20)$$

$$\eta_{\mathrm{graded}} = \frac{(mL_n+\gamma_n)(G_2-G_1)+NL_n(G_2+G_1)}{(mL_n+\gamma_n)\sinh(NW_p)+NL_n\cosh(NW_p)}\frac{\mathrm{e}^{mW_p}}{2} \quad . \quad (21)$$

In n-on-p graded HgCdTe homogeneous diodes the quantum efficiency and photogenerated current dominate the detection ability under room temperature. The built-in electric field $\varepsilon_{\mathrm{built-in}}$ due to the grading of energy bandgap grading across the p-type graded region has direct effect on response time of the photodiode. The total response time of photodetectors includes the diffusion time t_{absorber} in the graded bandgap HgCdTe absorption layer and the transit time in the drift layer t_{transit}. The frequency response of n-on-p HgCdTe photodetector is limited by electron transport time and 3dB bandwidth of the device can be calculated, the diffusion time and transit time should be given as

$$\frac{1}{t_{\mathrm{absorber}}} = \frac{1}{t_{\mathrm{diffusion}}} + \frac{1}{t_{\mathrm{built-in}}} \quad , \quad (22)$$

$$t_{\mathrm{diffusion}} = \frac{W_p^2}{D_n} \quad , \quad (23)$$

$$t_{\mathrm{built-in}} = \frac{W_p}{\mu_n \varepsilon_{\mathrm{built-in}}} \quad , \quad (24)$$

$$t_{\mathrm{transit}} = \frac{w_n}{v_n} \quad , \quad (25)$$

where $\mu_n$is the electron mobility under the electric field and v_n is the carrier velocity before enter the drift layer, w_n is the thickness of drift layer, which is formed by ion implantation in p-n junction. The one-dimensional equations based on analysis of graded HgCdTe photodetectors agree well with the optical and electrical performance of graded photodiodes. The built-in electric field induced by composition grading in p-type region has effects on quantum efficiency and response time, which is further confirmed by devices fabricated by LPE and VPE HgCdTe materials. The model is consistent with the measured result, which indicates the accuracy of the fixed model based on n-on-p graded structure.

3 Device photoresponse performance under laser illumination

The impulse and frequency response of the graded HgCdTe photodetectors is further investigated. Figure 3(a) illustrates the experimental setup for measurement of impulse response. The impulse response is induced by a semiconductor laser, which is capable of generating pulses with a full-width of 100 fs at a wavelength of 1.55 μm. Repetition frequency of pulses is 80 MHz. The response time of the MWIR HgCdTe photodetector can be measured by the curve extracted from the ultrafast oscilloscope. The HgCdTe photodetector is packaged in Dewar at room temperature, the curve is recorded with a sampling oscilloscope using a 20-GHz-BW sampling module. Figure 3(b) displays another way to measure the frequency response of ultrafast photodetector based on vector network analyzer and Lightwave Component Analyzer (LCA). The device is tested under dark and illumination conditions, and the high-speed response of device is examined by the LCA with an internal laser source and network analyzer over a frequency range from 50 MHz to 1 GHz. A modulated optical signal at a wavelength of 1550 nm with an average power of 5 mW is emitted from the LCA, and it is coupled into the device in sequence. The electrical output is measured through a low noise amplifier and a radiofrequency microwave probe. It could cause strong absorption at the surface of device given the large absorption coefficient at 1550 nm, and the frequency response of the device was analyzed, such as the S_{21} parameter of the network analyzer.

Figure 3(c) shows the relative light response of LPE graded n-on-p photodetector measured by using the LCA and high-speed network analyzer. The photodetector exhibits a 3dB bandwidth of 115 MHz, which is calculated by $f_{3\mathrm{dB}} = 1/t_{\mathrm{total}}$. Figure 3(d) depicts the relative light response of the VPE graded n-on-p photodetector and the 3dB bandwidth is approximately 750 MHz. The difference of measured frequency response of the LPE and VPE photodetector shows that the composition gradient induced built-in electric field has direct effect on transport of generated minority carriers. The measurement is under zero-bias voltage at room temperature, and the excellent frequency response performance of HgCdTe photodetector confirms that the built-in electric field can be used to optimize the design of ultrafast MWIR HgCdTe photodetector. Figure 3(e) and Fig. 3(f) depict the photoresponse of the LPE and VPE HgCdTe photodetector at a wavelength of 1 550 nm emitted by a femtosecond pulse laser with the pulse width of l00 femtosecond, respectively. The device can keep up with the fixed pulse frequency of the 1 550 nm laser, and the impulse responses measured at zero-bias voltage are characterized by the ultrafast oscilloscope. The LPE and VPE HgCdTe photodetectors show a fast rise time and a slower exponential fall time. The latter is correlated with the diffused photogenerated carriers in absorber region. The impulse response measurement corresponds well with the frequency response test. Figure 3(g) and Fig. 3(h) shows the photoresponse characteristics of the LPE and VPE photodetector when the incident light is repeatedly turned on and off at 2 000 nm. When the laser is turned on and off, the devices exhibit high and low current states, and the states are matched with the impulse laser. The devices show excellent stability and reliability even under laser after hundreds of seconds. In short, the response time of the photodetector based on graded bandgap structure is improved by a larger composition gradient induced built-in electric field, which can verify the validity of the model mentioned above. *A* quantitative comparison is presented in Table 1.

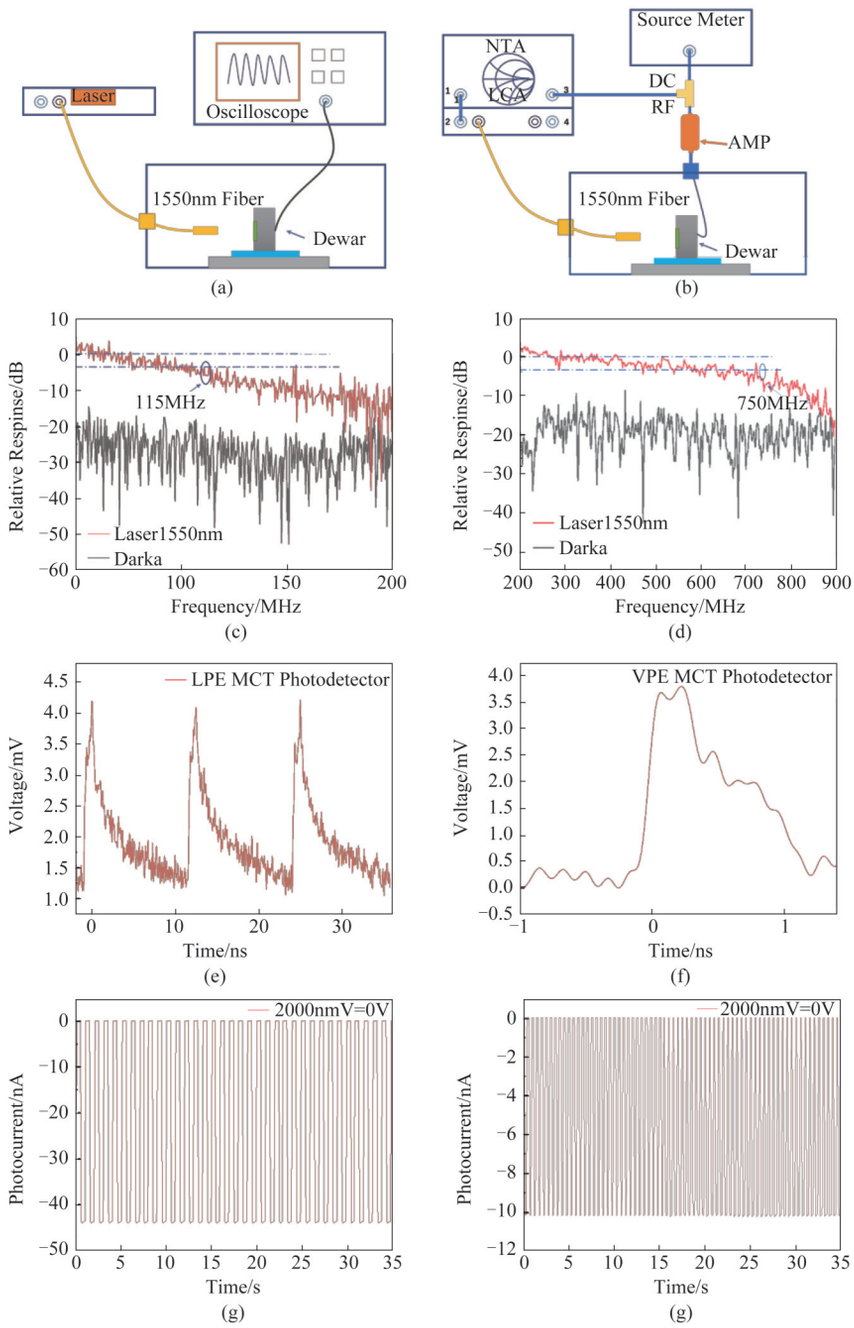

Fig. 3 Optoelectronic properties and frequency response of graded HgCdTe photodetectors under laser illumination at room temperature (**a**) impulse response measurement setup schematics for characterization of ultafast photodetectors, (**b**) lightwave Component Analyzer (LCA) and network analyzer setup for bandwidth characterization of high-speed photodetecto. (**c**) relative response versus switching frequency of LPE n-on-p photodetector, showing the 3 dB cutoff frequency of 115 MHz, (**d**) the relative response as a function of light intensity modulation frequency of VPE n-on-p photodetector, showing the 3 dB cutoff frequency of 750 MHz, (**e**) time response of the LPE photodetector under 1550 nm femtosecond pulse laser with the pulse width of l00 femtosecond. The repetition frequency of pulse is 80MHz and the analog output signal of LPE photodetector under pulse laser is measured, the curve is extracted from a highspeed oscilloscope, (**f**) time response of the VPE photodetector under 1550 nm femtosecond pulse laser, (**g**) time response curve of the LPE photodetector under 2000 nm switching conditions at U_{bias}= 0 V, (**h**) the time-resolved photoresponse curves of the VPE photodetector at room temperature under conditions of U_{bias}= 0 V.

图3 室温下测试HgCdTe器件的光电特性和频率响应表征 (a) 用于表征高速器件的时域脉冲响应的设备原理图，(b) 用于表征高速器件频域带宽的光波成分分析仪（LCA）和网络分析仪原理图，(c) 3 dB截止频率为115 MHz的LPE n-on-p碲镉汞器件的响应与频率的关系图，(d) 3 dB截止频率为750 MHz的VPE器件的响应与调制频率关系图示，(e) LPE碲镉汞器件在重复频率80 MHz及脉冲宽度为l00 fs的1550 nm激光下的时域响应，(f) VPE碲镉汞器件在激光下的时域响应，(g) 零偏下LPE器件在2 μm纳秒激光下的开关特性，(h) 零偏下VPE器件的开关特性

Table 1 Comparison of device performance for commercially available and reported MWIR HgCdTe ultrafast photodetectors
表1 已报道的MWIR碲镉汞高速光电探测器的器件性能比较

Material and Structure	Operation Temperature	Wavelength / μm	Responsivity or Quantum Efficiency	Response Time	Calculated Bandwidth	Reversed Bias Voltage	References
HgCdTe p-i-n	77 K	10	30 %		1 GHz	1. 5 V	[9]
HgCdTe APD	77. 3 K	5		5. 0 ns	145 MHz	12. 5 V	[10]
HgCdTe APD		5. 2		More than 1 ns	600 MHz	12 V	[11]
HgCdTe APD		1. 55		1. 5 ns	600 MHz	28 V	[12]
HgCdTe APD		4. 3			6. 8 MHz	11 V	[13]
MCT PV	300 K	4	2 A/W		6. 7 MHz		VIGO
MCT PV	300 K	4	1 A/W		8. 3 MHz		VIGO
MCT PV	300 K	5	1 A/W		8. 3 MHz		THORLABS
This Work	300 k	4	0. 3 A/W	1. 33 ns	750 MHz	0 V	

4 Conclusion

In summary, a high-speed room-temperature mid-wave infrared HgCdTe photodetector based on graded bandgap structure is demonstrated. LPE and VPE MWIR HgCdTe photodetectors are designed and fabricated, the devices depict excellent photoresponse at zero bias, showing frequency response of 115 MHz and 750 MHz, which corresponds the measurement under ultrafast impulse laser. The improvement of fast response can be attributed to a larger built-in electric field result from the graded composition gradient in n-on-p structure. Moreover, the analysis based on one-dimensional equations illustrates the influence of graded bandgap on quantum efficiency and response time. The impulse responses of LPE and VPE HgCdTe photodetectors are compared to confirm the validity of one-dimensional model. The improved graded bandgap designs promise faster photoresponse for the detector, which is reliable for ultrafast photonic applications under zero bias and operated at room temperature.

References

[1] Konstantatos G, Sargent E H. Nanostructured materials for photon detection[J]. *Nature nanotechnology*, 2010, **5**(6):391-400.
[2] Schliesser A, Picqué N, Hänsch T W. Mid-infrared frequency combs [J]. *Nature photonics*,2012, **6**(7):440-449.
[3] Galli I, Bartalini S, Cancio P, *et al*. Mid-infrared frequency comb for broadband high precision and sensitivity molecular spectroscopy [J]. *Optics letters*, 2014, **39**(17):5050-5053.
[4] Luzhansky E, Choa F S, Merritt S, *et al*. Mid-IR free-space optical communication with quantum cascade lasers[J]. *Laser Radar Technology and Applications XX; and Atmospheric Propagation XII. SPIE*, 2015, **9465**:267-273.
[5] Liu C, Zhai S, Zhang J, *et al*. Free-space communication based on quantum cascade laser[J]. *Journal of Semiconductors*, 2015, **36**(9): 85-88.
[6] Rogalski A. HgCdTe infrared detector material: history, status and outlook[J]. *Reports on Progress in Physics*, 2005, **68**(10):2267.
[7] Reine M B. Review of HgCdTe photodiodes for IR detection[J]. *Infrared Detectors and Focal Plane Arrays VI. SPIE*, 2000, **4028**: 320-330.
[8] YE Zhen-Hua, LI Hui-Hao, WANG Jin-Dong, *et al*. Recent hotspots and innovative trends of infrared photon detectors [J]. *J. Infrared Millim. Waves*, (叶振华,李辉豪,王进东,等。红外光电探测器的前沿热点与变革趋势。**红外与毫米波学报**)2022, **41**(1): 15-39.
[9] Verie C, Sirieix M. Gigahertz cutoff frequency capabilities of CdHgTe photovoltaic detectors at 10.6 μm[J]. *IEEE Journal of Quantum Electronics*, 1972, **8**(2):180-184.
[10] Rothman J, Perrais G, Destefanis G, *et al*. High performance characteristics in pin MW HgCdTe e-APDs[J]. *Infrared Technology and Applications XXXIII. SPIE*, 2007, **6542**:475-484.
[11] Perrais G, Derelle S, Mollar D L, *et al*. Study of the transit-time limitations of the impulse response in mid-wave infrared HgCdTe avalanche photodiodes[J]. *Journal of Electronic Materials*, 2009, **38** (8):1790-1799.
[12] Rothman J, Foubert K, Lasfargues G, *et al*. Response time measurements in short-wave infrared HgCdTe e-APDs[J]. *Journal of Electronic Materials*, 2014, **43**(8):2947-2954.
[13] Beck J, Welch T, Mitra P, *et al*. A highly sensitive multi-element HgCdTe e-APD detector for IPDA lidar applications[J]. *Journal of Electronic Materials*, 2014, **43**(8):2970-2977.
[14] Tobin S P, Hutchins M A, Norton P W. Composition and thickness control of thin LPE HgCdTe layers using x-ray diffraction[J]. *Journal of Electronic Materials*, 2000, **29**(6):781-791.
[15] Dhar V, Bhan R K, Ashokan R. Effect of built-in electric field on crosstalk in focal plane arrays using HgCdTe epilayers[J]. *Infrared Physics & Technology*, 1998, **39**(6):353-367.
[16] Hu W D, Chen X S, Yin F, *et al*. Analysis of temperature dependence of dark current mechanisms for long-wavelength HgCdTe photovoltaic infrared detectors[J]. *Journal of Applied Physics*, 2009, **105** (10):159.
[17] Daraselia M, Carmody M, Edwall D, *et al*. Improved model for the analysis of FTIR transmission spectra from multilayer HgCdTe structures[J]. *Journal of Electronic Materials*, 2005, **34**(6):762-767.
[18] Rosenfeld D, Garber V, Bahir G. The effects of built-in electric field on the performance of compositionally graded P-on-n HgCdTe heterojunction photodiodes[J]. *Journal of Applied Physics*, 1995, **77**(2): 925-933.
[19] Ariel V, Garber V, Rosenfeld D, *et al*. Estimation of HgCdTe bandgap variations by differentiation of the absorption coefficient[J]. *Applied Physics Letters*, 1995, **66**(16):2101-2103.
[20] Schmit J L. Growth, properties and applications of HgCdTe[J]. *Journal of Crystal Growth*, 1983, **65**(1-3): 249-261.